J Mater Sci (2008) 43:4658–4665
DOI 10.1007/s10853-008-2668-0

High energy impact techniques application for surface grain refinement in AZ91D magnesium alloy

Li-feng Hou · Ying-hui Wei · Bao-sheng Liu · Bing-she Xu

Received: 22 August 2007 / Accepted: 21 April 2008 / Published online: 13 May 2008

Abstract A nanostructured surface layer was fabricated on magnesium alloy AZ91D by using the high-energy impact technique (HEIT). With the help of transmission electron microscope (TEM) and high-resolution transmission electron microscope (HRTEM), the microstructure features of the surface layer were systematically observed and characterized in different stages of microstructure evolution. The result revealed the mechanism of grain refinement and strain accommodation. The process of grain refinement, accompanied by an increase in strain in the surface layer, resulted from several processes. The onset of $\{01\bar{1}2\}$ deformation twinning and the intersection with $\{10\bar{1}1\}$ twins system are one of them. The operation of $\langle 11\bar{2}0\rangle(0001)$ basal slip and $\langle 11\bar{2}3\rangle(1\bar{1}02)/(0\bar{1}1\bar{2})$ pyramidal slip led to the formation of dislocation cells and low-angle dislocation boundaries. The successive subdivision of grains to a finer scale resulted in the formation of highly disoriented nanocrystalline grains. The mechanism of grain refinement was interpreted in terms of the structural subdivision of grains together with dynamic recrystallization. The minimum size of such refined grains was about 40 nm.

L.-f. Hou · Y.-h. Wei (✉) · B.-s. Liu · B.-s. Xu
College of Materials Science and Engineering,
Taiyuan University of Technology, Taiyuan 030024,
People's Republic of China
e-mail: yhwei@public.ty.sx.cn

L.-f. Hou · Y.-h. Wei · B.-s. Xu
Key Laboratory of Interface Science and Engineering
in Advanced Materials of Taiyuan University of Technology,
Ministry of Education, Taiyuan 030024,
People's Republic of China

Introduction

Grain refinement induced by severe plastic deformation (SPD) in metallic materials has been a subject of many researches in the last decade [1–3]. The principle of SPD is that it based on imposing very large strains in the sample and the rearrangement of the dislocations induced by straining leads to very substantial grain refinement down to, typically, the submicrometer or even the nanometer scale [4]. The widely used SPD methods are equal-channel angular processing (ECAP), high-pressure torsion (HPT), and high-energy impact technique (HEIT). Among those methods, HEIT is the one of the most effective processing methods to fabricate various ultra fine-grain structures by imposing intense plastic strains onto the surface of the metals or alloys. This technique successfully achieved a gradient variation of plastic strains and strain rates in the sample from the treated top surface to the deep matrix. The microstructure observations at various depth levels can in turn provide the clue to the process of structural evolution relevant to various stages of strain.

Compared with other conventional treatments such as impact [5–8], there are several different aspects. The HEIT uses much larger balls (a few mm) than the projectiles in the impact (1–3 mm in diameter). Spherical balls with smooth surface are essential for obtaining a nanostructural surface layer in the HEIT. Balls with rough surface, as in impact technique, will damage the surface layer during the HEIT treatment. The velocity of the balls in the HEIT process is much lower (1–20 m/s) compared with the conventional impact technique (typically about 5 km/s and above). Conventional impact technique is a directional process in which the angle between the shot jet and the sample surface is normally fixed at 90° in many cases. In contrary, the HEIT requires random directional impacts of

the balls onto the sample to facilitate the grain refinement process. The strain rates in conventional impact technique are also much higher (10^5 s^{-1}) [9] compared with the HEIT (10^2–10^3 s^{-1}).

As of now, the ultra fine-grain or nanocrystalline specimens have been fabricated in several metal materials such as iron [10], low carbon steel [11], stainless steel [12, 13], and titanium [14] with the help of HEIT. In related works with this article, nanocrystalline microstructures have also been fabricated in aluminum alloys [15, 16], cobalt [17], Zr [18], etc. Most documented experiments and theoretical studies show that the grain refinement results from dislocation activities during deformation in cubic (face-centered cubic (fcc) and body-centered cubic (bcc)) metals and alloys with a medium to high stacking fault energy (SFE). In contrast, the low SFE fcc materials exhibit a different mode of grain refinement, which involves the slip of dislocation and subsequent deformation twinning, followed by interplay of twins with dislocations. As for the hexagonal close packed (hcp) metals, deformation twinning occurs at the early stage of deformation and serves as an additional deformation mechanism to dislocation slip [17].

Mg-based alloys have excellent strength to weight ratio, which makes it good for applications such as structural components in automobile and aircraft industries [19]. But Mg alloys have low strength and ductility compared to aluminum alloys. It is due to their hcp structure with limited slip systems. Recent studies have demonstrated that Mg alloy with an ultra fine-grain structure in submicrometer range can be processed using SPD methods such as ECAP, which offers a simple and effective way to increase the mechanical properties of magnesium alloys [20–25]. However, in most of these cases, the strain rate $\dot{\varepsilon}$ was $<10^{-1}$ s^{-1} and the grain size of the final refined structure was in the scale of micrometers or submicrometers. From those studies, it is not clear what dominates the grain refinement process and weather grain size can be further fine tuned into nanometer range.

In the present study, we have examined the microstructure changes in the various layers of AZ91D magnesium alloy with the HEIT treatment. The HEIT process has been proved to be able to produce nanocrystalline structure in the surface of most metals. The approximate strain rate is 10^2–10^3 s^{-1} near the top treated surface, scaling down to zero in the deep matrix. Consequently, a gradient microstructure is obtained in the sample, due to different levels of strain rate and different degrees of plastic strain. This provides a unique opportunity to characterize deformation mode of the Mg alloy over a wide range of strain rates and to understand the corresponding grain refinement mechanisms by examining the microstructure features at different depths of a single-treated sample.

Experimental

The material used in the present study is the commercial AZ91D plate with a chemical composition (mass fraction, %) of 8.63Al, 0.66Zn, 0.29Mn, balance Mg. The alloy plate was cut into pieces with dimension of 100 mm × 100 mm × 5 mm suitable for HEIT processing. The alloy was solution heat-treated for 18 h at temperature of 413 °C. Microscopic examination revealed an initial grain size in order of ~150 μm. A smooth surface was attained by polishing with 700-grade SiC paper. During HEIT process, hardened stainless steel balls of 6 mm in diameter were placed at the bottom of a vacuum chamber which was attached to a vibration generator. Because of the high vibration frequency of the system, the sample surface to be treated was impacted, respectively, by a large number of balls within a short-time period. Each impact results in plastic deformation in the surface layer of the treated sample. As a consequence, surface nanocrystallization was conducted on the sample. In this work, the treatment lasted for 30 min, with a vibrating frequency of 50 Hz under vacuum.

The X-ray diffraction analysis was done on a Rigaku D/MAX2400 X-ray diffractometer with CuK_α radiation. H-800 transmission electron microscope (TEM) and JEOL-2010 high resolution transmission electron microscope (HRTEM) were used to examine the microstructures at the different depths ranging from the surface to the matrix. The plane view TEM foils of layers at different depths were obtained by first polishing the corresponding surface layer; then mechanically grinding the sample on the untreated side down to about 30 μm thick; finally ion milling the untreated side of thin foils at room temperature in a Gatan PIPS with a small incident angle. A MVK-H3 Vickers hardness testing machine was used to examine the variation of hardness along the sections perpendicular to the treated surface of the specimens.

Experimental results

TEM investigation

Deformation twinning (~250 μm below the treated surface)

Figure 1a is a cross-sectional bright-field transmission electron microscope (TEM) micrograph of the microstructure at about 250 μm depth below the treated surface. The deformation twinning with straight boundary does generally run across the entire length in the grain and stop at the grain boundary. Figure 1b shows selected area electron diffraction (SAED) patterns taken from areas that

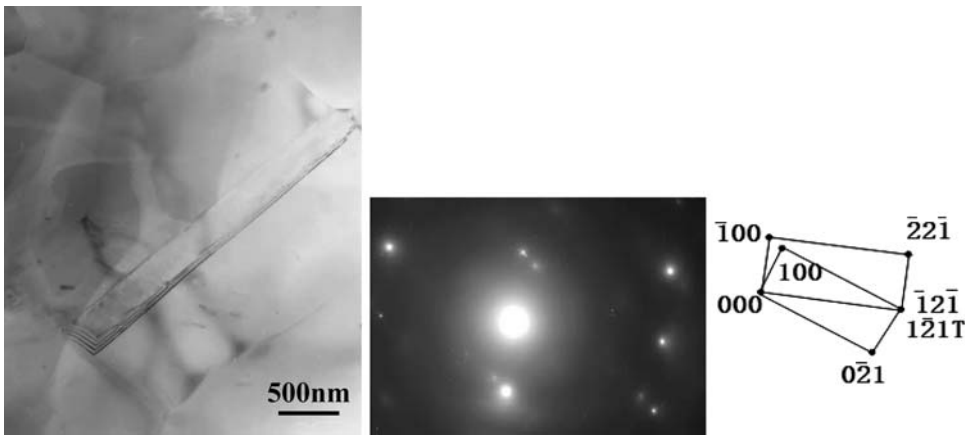

Fig. 1 (**a**) Bright-field TEM image showing the deformation twinning in the region that is 250 μm below the treated surface of AZ91D alloy, (**b**) corresponding SAED pattern and indexation

contain adjacent bands. This illustrates the twin relationship with twin plane $\{01\bar{1}2\}$ and twin direction $[\bar{1}2\bar{1}\bar{1}]$, indicating a $\{10\bar{1}2\}$ twin system.

A larger number of parallel and intersected bands were observed at the same depth of treated surface (Fig. 2). Their boundaries are not as straight as those of twins in Fig. 1. The angle between the interacting sections remains same for different twins shearing at the same or different time [26]. With the measured angle $50° \pm 7$, it can be concluded that the twin system is $\{01\bar{1}2\}$ and $\{10\bar{1}1\}$ twinning. That is the dominant mechanism of plastic deformation of AZ91D at the initial stage of HEIT process.

Dislocations slipping ($\sim$120 μm below the treated surface)

Transmission electron microscope examination of the layer about 120 μm below the surface shows that the microstructure differs considerably from that observed at the depth of 250 μm. The series of straight and parallel dislocations have been found in the grain (shown in Fig. 3). These images were taken with an incident electron beam direction of $[11\bar{2}0]$ under a two-beam diffraction condition with different $\vec{g}$. In Fig. 3a, the dislocations are visible, but invisible in Fig. 3b and c. With the $\vec{g} \cdot \vec{b}$ criterion, all the observed dislocations were found to be of $\langle a \rangle$ type, $\vec{b} = (1/3)\langle 11\bar{2}0 \rangle$. Most dislocation segments are parallel to the basal plane trace, as indicated by a single arrow. They are basal $\langle a \rangle$ dislocations for the basal slip. Moreover, a lot of dislocation pile-ups in or near the grain boundaries have also been found, as shown in Fig. 4. The dislocations arrangement in the network becomes more complex. The average dislocation spacing in the network is measured at about tenths of nanometers (Fig. 4). Under a two-beam diffraction condition, using the $\vec{g} \cdot \vec{b}$ criterion, most dislocations were found to be $\langle a + c \rangle$ type, $\vec{b} = (1/3)\langle 11\bar{2}3 \rangle$.

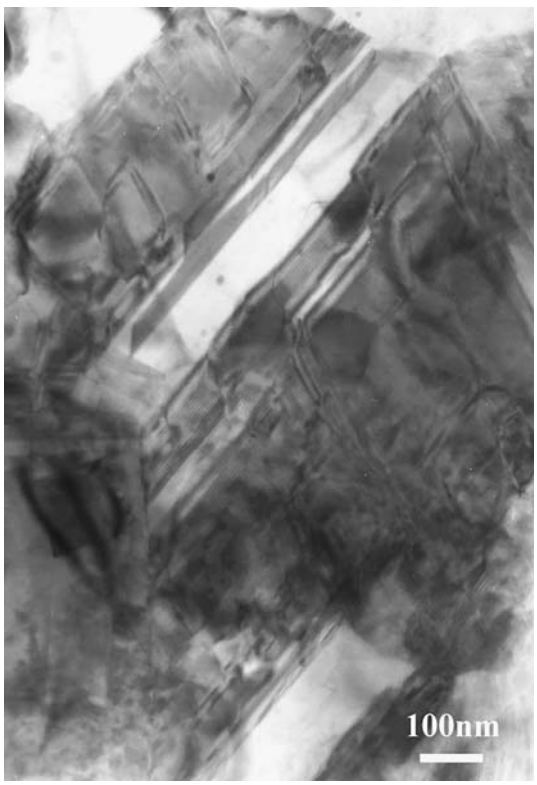

Fig. 2 Bright-field TEM image showing the interlaced lamellae

Besides, these dislocations appear to be on the $(1\bar{1}02)$ and $(0\bar{1}1\bar{2})$ pyramidal planes for the pyramidal slip. The dominant mechanism of plastic deformation is the basal $\langle a \rangle$ dislocation slip and pyramidal $\langle a + c \rangle$ dislocation slip. A lot of dislocations arrayed in networks indicated that considerable recovery has also occurred. A few of dislocations cells are formed in grains by the dislocation slipping, as indicated by a single arrow in Fig. 5. The boundary between the dislocation cells is of low angle indicated by a single arrow. Figure 6 shows the microstructure of dislocation cells in the grain.

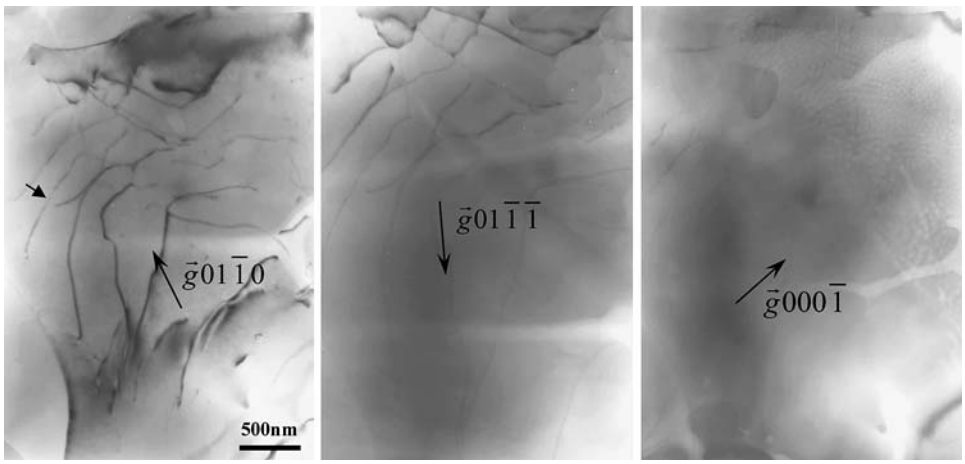

Fig. 3 Bright-field TEM images showing the straight dislocations in the grains. Contrast analysis of dislocation configuration under $\vec{g} = 01\bar{1}0$ (**a**), $\vec{g} = 01\bar{1}\bar{1}$ (**b**), $\vec{g} = 000\bar{1}$ (**c**), respectively

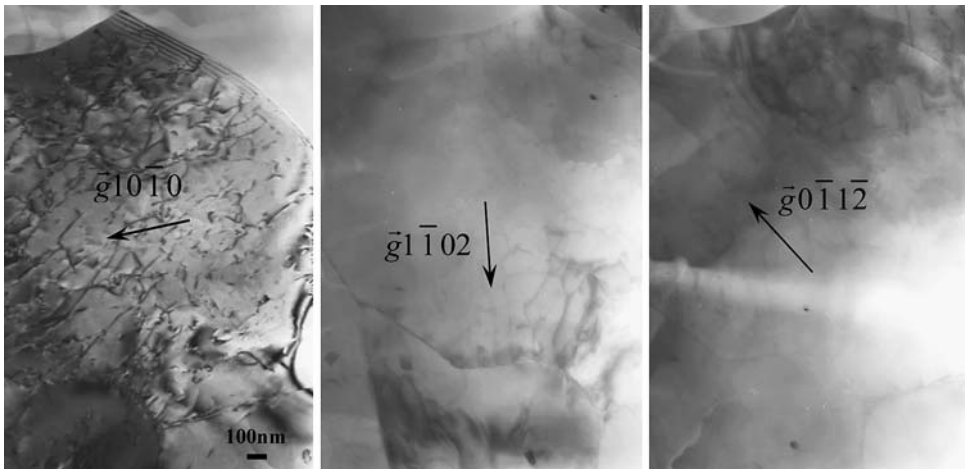

Fig. 4 Bright-field TEM image showing a lot of dislocation pile-ups present on or near the boundaries

Subgrain (∼60 μm below the treated surface)

Transmission electron microscope examination of the layer about 60 μm below the surface of specimen shows that the microstructure also differs considerably from that observed at the depth of 120 μm. This is the submicrometer region due to the higher stress and strain compared with the previously deformed region, in turn, with increased density of the dislocation pile-ups in the alloy. Figure 7 shows typical dislocation arrangements in the alloy. A lot of dislocation pile-ups can be found. The spacing between each parallel dislocation in the pile-ups is measured to be only several nanometers. The length of the dislocations in the pile-ups is about tens of nanometers. At the same time, the TEM micrograph in Fig. 7 shows the grain sizes are about 200 nm (about 60 μm deep below treated surface), finer than the grains showed in Fig. 6.

Nanograin (∼20 μm below the treated surface)

An examination of the top surface layer of specimen (20 μm below the treated surface) shows that the microstructure is uniformly distributed nanometer-scale grains (Fig. 8). The TEM micrograph illustrates the equiaxed microstructure in the nanometer region. The average grain size is determined to be ∼40 nm. The corresponding SAED pattern is also presented. The ring-like electron diffraction pattern shows that grain orientation is random, which indicates highly disoriented boundaries.

Figure 9 shows a HRTEM micrograph of the layer in a depth of about 20 μm from the top surface layer of sample after HEIT treatment for 30 min. It shows that these grains have stacking fault (indicated by arrowhead) and dislocation (showed in circle) in their interior even at their initial stage of formation.

Hardness variation

Figure 10 shows the micro hardness variation along the depth from the treated surface of the sample by HEIT treatment for 30 min. Compared with that of the matrix of sample, the microhardness of the top surface nanocrystalline layer is about three times that of the coarse-grains matrix. The hardness of the layer at 40 μm below the

Fig. 5 Bright-field TEM image showing the dislocations arrayed in networks and a few of dislocations cells formed

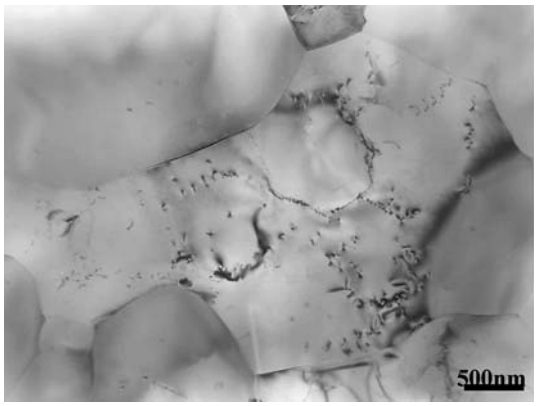

Fig. 6 TEM image showing the dislocation cells in the grain

surface is increased too. With the further increase in depth, the hardness variation tends to be steady. The increase of the surface hardness of the sample after HEIT treatment is attributed to the grain refinement. Moreover, the stacking fault and dislocation seem to occur preferentially in smaller grains and propagates across the entire grain, which was one of the reasons for the surface having higher hardness than the inside. So it can be concluded that the surface nanocrystalline helps to strengthen the surface materials.

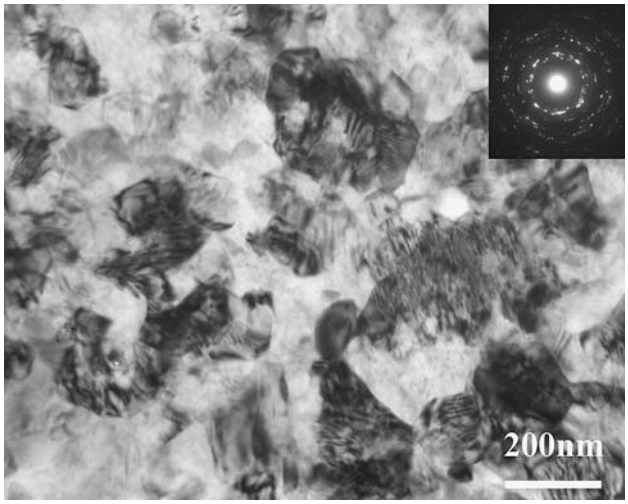

Fig. 7 TEM image of the subgrains, there is a lot of dislocations pile-ups in the grain

Discussions

On the basis of the microstructure features observed at various depths and different levels of strain in the deformed surface layer, it can be concluded that, as the strain and strain rate increase, the following changes occur in the microstructure of Magnesium alloy during HIET, the details of which are discussed below:

(1) The onset of twins and the interaction of twin systems.
(2) The slipping of dislocations at $\langle a \rangle$ type and $\langle a + c \rangle$ type.
(3) The formation of dislocation cells, and change to the subgrains.
(4) The further breakdown of submicronic polygonal grains into randomly oriented nanograins by dynamic recrystallization (DRX).

Onset of twins and the slipping of dislocations

Five independent slip systems are necessary for polycrystalline materials to undergo homogenous plastic deformation [27]. Most magnesium alloys are of hcp structure. The mechanism of plastic deformation is basal slip, prismatic slip, pyramidal slip and twinning. At room temperature, the critical resolved shear stress (CRSS) of the prismatic and pyramidal slip was higher than basal slip. So only two independent slip systems consist of the basal plane and three close-packed directions can accommodate vertical to the c axes [28–30]. The twinning planes in magnesium are $\{10\bar{1}2\}$, $\{10\bar{1}1\}$, $\{11\bar{2}2\}$ and $\{11\bar{2}1\}$ depending on the temperature and deformation conditions [31]. It has been observed that the twinning is the prevalent

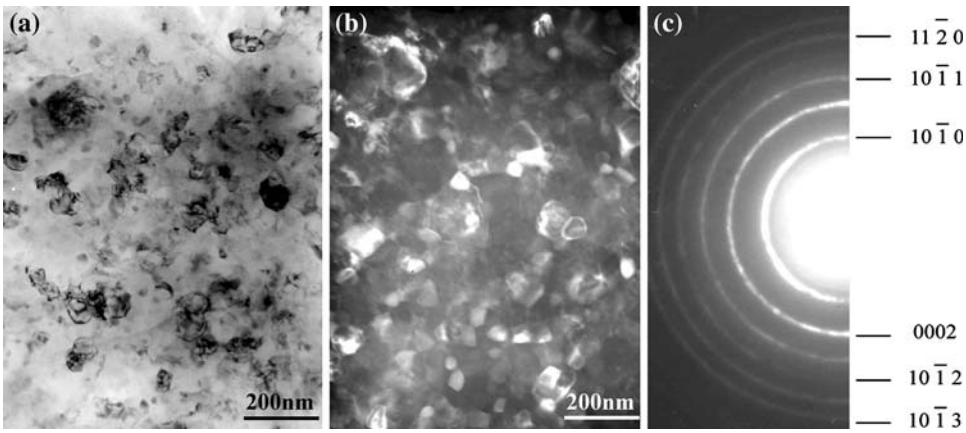

Fig. 8 Figures (**a**) and (**b**) correspond to bright and dark images taken from surface layer (about 20 μm thick) of the treated sample showing the equiaxed nanograins; (**c**) is the corresponding SAED pattern

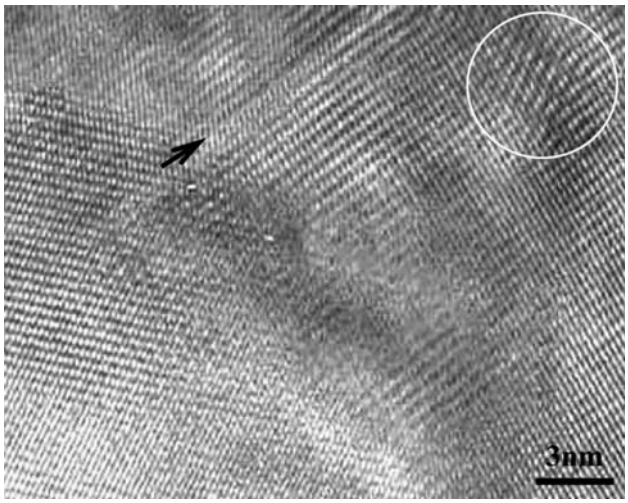

Fig. 9 HRTEM image of the nanocrystalline grains. The stacking fault marked by a single arrow; the dislocation marked by the circle

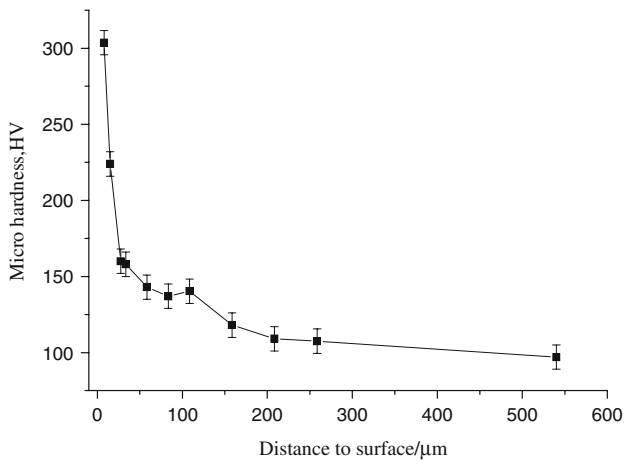

Fig. 10 Hardness evolution along the depth of the sample HEIT treated for 30 min

deformation mode at low strain in the layer adjacent to the substrate. The twinning plane observed in our study is of the $\{10\bar{1}2\}$ type, one of the most frequent at ambient temperature. Multidirectional repetitive loading and increasing strain facilitate the interaction and the initiation of different twin systems, leading to their interaction, such as $\{01\bar{1}2\}$ and $\{10\bar{1}1\}$. Since the deformation is limited to deformation twinning, the gross deformation produced by twins is quite small and most of the plastic strain is due to movement of the dislocations [32]. In the experiment, the twins are not produced at various strain rates at all during the deformation. The twins appear only in the layer in which the strain is low. It implies the twinning, which divides the original coarse grains into finer twin platelets, governed the plastic deformation at the beginning.

As the strain increases, the further formation of twins will reduce the scale of the microstructure. The dislocation activity will then predominate. The presence of twins and their interaction or the grain boundaries hinder dislocation activity movement. Hence, a high dislocation density occurs at twin boundaries and the grain boundaries, as shown in Figs. 3 and 4. The TEM images indicate that the dominant deformation mechanism for the sample is basal $\langle a \rangle$ slip and pyramidal $\langle a + c \rangle$ slip. Commonly, the pyramidal slip was difficult to produce at the ambient temperature because the CRSS of pyramidal slip is considerably higher than the basal slip. However, in magnesium alloys the pyramidal slip can occur at the place where the stress concentrated, such as grain boundaries [33]. In addition, the temperature in the treated layer will rise due to repetitive peening of balls during HEIT process and hence the pyramidal slip would be apt to occur. Moreover, the dislocation loops are visible in the grains, as shown in Fig. 11, which indicated that the dislocations were cross-slip and left behind the dislocations loop in the area without the dislocations [34].

Subdivision of grain and formation of a nanostructure

As the increase of the strain, the dislocations are rearranged to minimize the total system energy. The dislocation cells

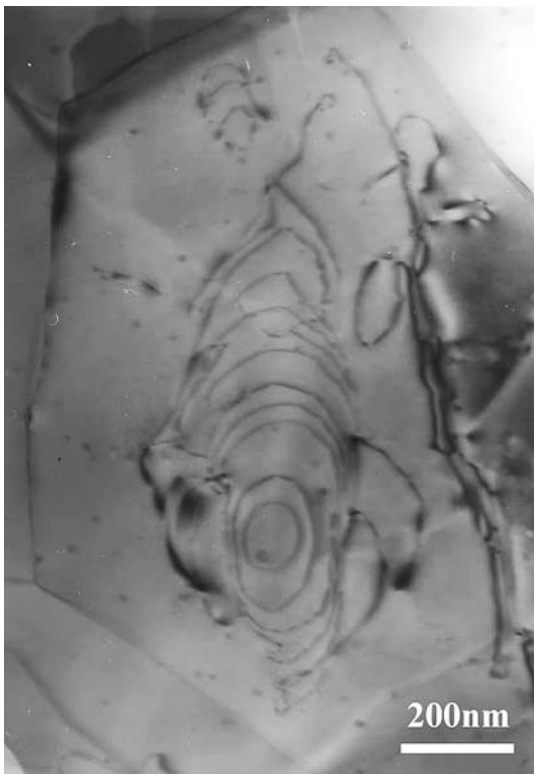

Fig. 11 Bright field image showing the dislocation loops

were formed inside the grain in Figs. 5 and 6 corresponding to a typical configuration that can accommodate plastic deformation. This is the typical character of the dynamic recovery (DRV). It suggests that these dislocation cells are at the origin of the formation of subgrain boundaries which will subsequently be converted into low-disoriented angle blocks before becoming submicronic polygonal grains.

The formation of equiaxed nanograins was observed close to the top treated surface (Fig. 8). It can be seen that the grain boundaries are well delineated. The diffraction rings in Fig. 8 are more continuous than the rings in Fig. 7, which indicated the nanograins are of random orientations. It is likely that nanograins result from the further evolution of submicronic grains due to the very high strain and strain rate on the top surface. It can be assumed that a recrystallization process may play an important role in their formation. This hypothesis has been supported by Fig. 12, which showed the presence of DRX grains (marked by single arrows). It has been also observed that the dislocation density is often lower in DRX grains than it is in grain (Fig. 4). For AZ91D magnesium alloy the melting point is 871 K; the recrystallization often happens at the range of 0.5–0.6 Tm, with 0.5 Tm corresponding to 435.5 K. The DRX temperature could be even lower than this temperature, even at ambient temperature [35]. During the HEIT process, the repeated multidirectional impact of flying balls generates severe deformation and strain at very high strain

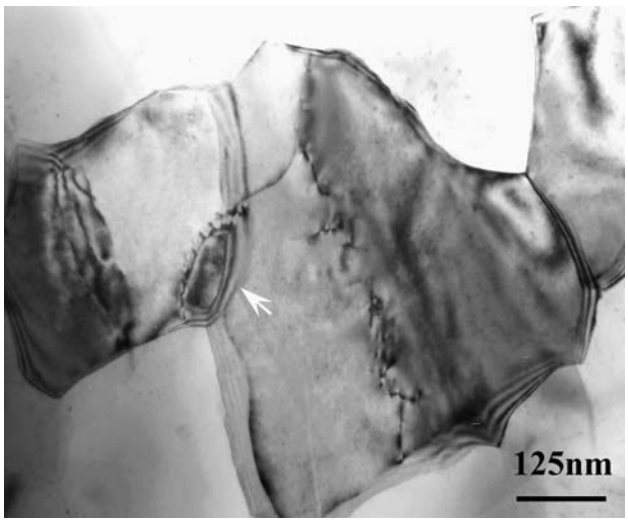

Fig. 12 TEM image of the subgrain

rate (about 10^2–10^3 s^{-1}) in the region near the top surface. In addition, the temperature in the treated layer will rise due to repetitive peening of balls during HEIT process. Therefore, the onset of a DRX event is easy to happen. Otherwise, the SFE of magnesium alloy is very low, especially the basal planes are only 10 mJ m^{-2} [36], which also increase the nucleation of DRX grains. Derby [37] has ever carried out a systematic analysis of DRX in relation to two mechanisms: nucleation and the growth of recrystallized grains in a deformed material (classical recrystallization) and the formation of recrystallization by the gradual rotation of subgrains (rotation recrystallization). Both mechanisms lead to the break-up of the original grain structure. In classical recrystallization, new grains are nucleated in area of high plastic strain and grow into the deformed material. In rotation recrystallization, rotation of the cells and subgrains occurs gradually until all the dislocations are absorbed by the grain boundaries. In the experiment, TEM examinations do not show evidence of nucleation and growth mechanism for nanograins but indicate clearly the importance of grain boundary rotation in microstructural development. It is suggested that rotation recrystallization may play a major role in the final grain refinement mechanism during HEIT process. Simultaneously, the disorientations of subgrains increase with strain and evolve into high angle boundaries through the dislocation regrouping. The process of grain subdivision may proceed successively to finer and finer scale with strain, resulting in the formation of ultra fine crystallites and nanocrystallizes.

Hence, the grains refinement mechanism of AZ91D magnesium alloy induced by HEIT treatment is the co-operation mechanisms, which are dislocation slipping and DRX operation simultaneously. The deformation

twinning plays the role of harmonizing the deformation at the initial stage.

Summary

An experimental study has been performed to document the grain refinement and strain accommodation in magnesium alloys subjected to the HEIT. In the experiment, the nanocrystalline layer is successfully fabricated on the surface of the AZ91D magnesium alloy by HEIT. The grain sizes range from about 40 nm at the top surface layer, gradually to more than 200 nm at a depth of about 60 μm, finally to ~150 μm at the matrix. The TEM investigations show the following changes in the initial coarse grain structure as the strain increases: (1) the onset of $\{10\bar{1}2\}$ twins and the interaction with $\{10\bar{1}1\}$ twin system, (2) The slipping of dislocations at $\langle a\rangle$ type and $\langle a+c\rangle$ type, (3) the formation of dislocation cells and change to the subgrains, (4) further breakdown of submicron polygonal grains into randomly oriented nanograins by DRX. Hardness measurements indicated a significant increment of hardness in the surface layer with nanostructures subjected to HEIT treatment compared with that of the matrix of sample. The microhardness of the top surface is about three times than that of the coarse-grained matrix.

Acknowledgements This research was supported by National Natural Science Foundation of China (50471070, 50644041), Shanxi Province Youth Science and Technology Foundation (20041023), and Shanxi Province Key Laboratory Opening Foundation.

References

1. Korznikov AV, Ivanisenko YV, Laptionok DV, Safarov IM, Pilyugin VP, Valiev RZ (1994) Nanostruct Mater 4:159. doi:10.1016/0965-9773(94)90075-2
2. Tao NR, Sui ML, Lu J, Lu K (1999) Nanostruct Mater 11:433. doi:10.1016/S0965-9773(99)00324-4
3. Shin DH, Kim BC, Kim YS, Park KT (2000) Acta Mater 48:2247. doi:10.1016/S1359-6454(00)00028-8
4. Yamashita A, Horita Z, Langdon TG (2001) Mater Sci Eng A 300:142. doi:10.1016/S0921-5093(00)01660-9
5. Rivas JM, Quinones SA, Murr LE (1995) Scripta Metall Mater 33:101. doi:10.1016/0956-716X(95)00105-5
6. Murr LE, Niou C-S, Garcia EP, E.Ferreyra ET, Rivas JM, Sanchez JC (1997) Mater Sci Eng A 222:118. doi:10.1016/S0921-5093(96)10518-9
7. Murr LE, Quinones SA, Ferreyra E, Ayala A, Valerio OL, Hörz F, Benhard RP (1998) Mater Sci Eng A 256:166. doi:10.1016/S0921-5093(98)00796-5
8. Francesconi A, Pavarin D, Giacomuzzo C, Angrilli F (2006) Int J Impact Eng 33:264. doi:10.1016/j.ijimpeng.2006.09.056
9. Murr LE, Shih HK, Niou C-S (1994) Mater Charact 33:65. doi:10.1016/1044-5803(94)90060-4
10. Tao NR, Wang ZB, Tong WP, Sui ML, Lu J, Lu K (2002) Acta Mater 50:4603. doi:10.1016/S1359-6454(02)00310-5
11. Liu G, Wang SC, Lou XF, Lu J, Lu K (2001) Scripta Mater 44:1791
12. Liu G, Lu J, Lu K (2000) Mater Sci Eng A 286:91. doi:10.1016/S0921-5093(00)00686-9
13. Zhang HW, Liu G, Hei ZK, Luu J, Lu K (2003) Acta Metall Sin 39:342
14. Zhu KY, Vassel A, Brisset F, Lu K, Lu J (2004) Acta Mater 52:4101. doi:10.1016/j.actamat.2004.05.023
15. Lanqing H, Ke W, Gang L, Bingshe X (2005) Trans Nonferrous Met Soc Chin 15:615
16. Wu X, Tao N, Hong Y, Xu B, Lu J, Lu K (2002) Acta Mater 50:2075. doi:10.1016/S1359-6454(02)00051-4
17. Wu X, Tao NR, Hong Y, Liu G, Xu B, Lu J, Lu K (2005) Acta Mater 53:681. doi:10.1016/j.actamat.2004.10.021
18. Caiyun S, Jijie X, Xiaolei W, Youshi H, Gang L, Jian L, Lu K (2004) Trans Mater Heat Treat 25:1242
19. Koike J, Ohyama R (2005) Acta Mater 53:1963
20. Yoshida Y, Cisar L, Kamado S et al (2003) Mater Sci Eng A 419–422:533
21. Kim WJ, Hong SI, Kim YS, Min SH, Jeong HT, Lee JD (2003) Acta Mater 51:3293. doi:10.1016/S1359-6454(03)00161-7
22. Kim WJ, Kim JK, Chao WY, Hong SI, Lee JD (2000) Acta Mater 48:2625. doi:10.1016/S1359-6454(00)00061-6
23. Yoshida Y, Cisar L, Kamado S (2003) Mater Trans 44:468. doi:10.2320/matertrans.44.468
24. Watanabe H, Mukai T, Kamado S, Kojima Y, Higashi K (2003) Mater Trans 44:463. doi:10.2320/matertrans.44.463
25. Matsubara K, Miyahara Y, Horita Z, Langdon TG (2003) Acta Mater 51:3037. doi:10.1016/S1359-6454(03)00118-6
26. Zhenhua C, Chunhua Y, Changqing H, Weijun X, Hongge Y (2006) Mater Rev 20:107
27. Von Mises R (1928) Angew Z Math Mech 8:161
28. Bohlen J, Chmelík F, Dobroň P, Letzig D, Lukáč P, Kainer KU (2004) J Alloys Compd 378:214. doi:10.1016/j.jallcom.2003.10.101
29. Staroselsky A, Anand L (2003) Int J Plasticity 19:1843. doi:10.1016/S0749-6419(03)00039-1
30. Jäger A, Lukáč P, Gärtnerová V, Bohlen J, Kainer KU (2004) J Alloys Compd 378:184. doi:10.1016/j.jallcom.2003.11.173
31. Yoo MH (1981) Metall Mater Trans A 12A:409
32. Courteny TH (1990) Mechanical behavior of materials. McGraw-Hill, New York
33. Yoo MH, Agnew SR, Morris JR, Ho KM (2001) Mater Sci Eng A 319–321:87
34. Puschl W (2002) Prog Mater Sci 47:415. doi:10.1016/S0079-6425(01)00003-2
35. Kaibyshev R, Sitdikov O (1994) Z Met Kd 85:738
36. Zhenhua C, Weijun X, Hongge Y, Dingfa F, Jihua C (2004) Chem Ind Eng Progress 23:127
37. Derby B (1991) Acta Metall Mater 39:955. doi:10.1016/0956-7151(91)90295-C